Accounts

Electrochemical Lithium Intercalation within Carbonaceous Materials: Intercalation Processes, Surface Film Formation, and Lithium Diffusion

Zempachi Ogumi* **and Minoru Inaba**

Department of Energy and Hydrocarbon Chemistry, Graduate School of Engineering, Kyoto University, Sakyo-ku, Kyoto 606-01

(Received July 31, 1997)

Electrochemical lithium intercalation within carbonaceous materials has attracted much attention for use to produce anodes in rechargeable lithium batteries. Although small-size rechargeable lithium cells using carbon anodes have been already commercialized, there still remain a lot of problems to be solved. Furthermore, recent global environmental issues require carbon anodes with high energy densities for use in electric energy storage and electric vehicles in the near future. This review article covers recent topics of the lithium intercalation, focusing on three fundamental aspects: intercalation processes, surface film formation, and lithium diffusion within carbons.

Carbonaceous materials are black (except diamond), odorless, tasteless, and nontoxic; they are used in a wide variety of industries. In the field of electrochemistry, different kinds of carbons have been used as electrode materials in industrial electrolyzers or conductive materials in batteries. However, they have never attracted as much attention from electrochemists as they do today. Excellent lithium intercalation properties, such as high reversible capacity and negative electrochemical potential close to metallic lithium electrode (Li/Li^+: -3.045 V vs. standard hydrogen electrode), make carbons very attractive candidates as anode materials for rechargeable lithium batteries.[1] The electrode reaction is described as:

$$C + xLi^+ + xe^- \underset{\text{Discharge}}{\overset{\text{Charge}}{\rightleftharpoons}} Li_xC. \quad (1)$$

Lithium is inserted within carbonaceous materials upon charging and extracted upon discharging of rechargeable lithium batteries.

The carbon anodes are combined with lithium-transition metal oxides such as $LiCoO_2$ as cathodes to form 4 V-class rechargeable lithium batteries, which have been commercialized in Japan since 1991. Since only lithium ions move from the cathode to anode upon charging, and vice versa upon discharging in this type of batteries, they are called "rocking chair-type" lithium batteries or "lithium-ion" cells.

A lot of carbonaceous materials have been manufactured and are commercially available. These include synthetic and natural graphite, cokes, carbon fibers, mesophase-pitch-based carbons, etc. Hundreds of these have been tested as anodes in lithium-ion cells. Furthermore, special carbons with additives, dopants, or substituents have been prepared and tested for this purpose. However, the answer to the question, "Which carbonaceous materials is the best?", has not been given yet. Although electrochemical lithium intercalation can be described in a simple electrochemical reaction as Eq. 1, it consists of various processes such as surface reactions, interfacial charge transfer reactions, and lithium diffusion inside the host carbon. Each of the elementary processes plays a vital role and greatly affects the charge and discharge characteristics of carbonaceous materials. Therefore, to understand the behavior of different carbonaceous materials, it is necessary to have a good understanding of each elementary process. Here the authors focus on three fundamental aspects of the intercalation: intercalation processes, surface film formation, and lithium diffusion, and summarize the results of recent studies on these aspects.

Structure of Carbonaceous Materials

Carbonaceous materials are classified into three allotropes: diamond, graphite, buckminsterfullerene.[2,3] Of these, only graphite and its disordered forms are practical materials for lithium-ion batteries. Graphite is a typical layered substance that consists of hexagonal sheets of sp^2-carbon atoms (called graphene layers), weakly bonded together by van der Waals forces into an ABAB$\cdots$ stacking sequence along the c-axis. The lattice belongs to a space group of $P6_3/mmc$, and the a- and c-axis lengths of the hexagonal unit cell are a_0=0.24614 nm and c_0=0.6708 nm, respectively, at room temperature. Graphite crystal thus has two kinds of characteristic surfaces,

normal and parallel to its *c*-axis; these are called basal and edge planes, respectively.

Although graphite exists in nature, it can be synthesized artificially by treating a pyrolyzed carbon at high temperatures around 3000 °C. While single crystal can be obtained in some cases, artificial graphite is usually polycrystalline. In addition to graphite, many kinds of carbonaceous materials such as carbon black, activated carbon, carbon fiber, cokes are manufactured. These artificial carbons are more or less disordered, and have some imperfections within them, such as stacking disorder of neighboring carbon layers, called "turbostratic disorder", and unorganized or buckled layers.[4] Carbonaceous materials heat-treated at lower temperatures are amorphous and are classified into two categories: "soft carbons (graphitizable carbons)" and "hard carbons (non-graphitizable carbons)".[4] In soft carbons, small crystallites are stacked nearly in the same direction, and thereby subtle diffusion induced by heat results in graphitization. In contrast, crystallites of hard carbons do not have such orientation and hence are difficult to develop even when heat-treated at high temperatures.

Anode Properties and Intercalation Processes of Different Carbonaceous Materials

As mentioned earlier, many kinds of carbonaceous materials have been tested as anodes in rechargeable lithium-ion batteries. The electrochemical characteristics of carbonaceous materials strongly depend on morphology, crystallinity, the orientation of crystallites, etc. In order systematically to understand the electrochemical properties of carbonaceous materials, it is convenient to classify them, first, into two categories, soft and hard carbons, and then to consider the effects of heat-treatment temperature (HTT). Figure 1 shows relationships between the specific capacity and HTT of soft and hard carbons, which were summarized by Dahn et al.[5] As shown in Fig. 1, soft and hard carbons show different variations with HTT. Graphite and highly graphitized carbons, which are prepared from soft carbons at temperatures >2400 °C, have specific capacities in the range 300—370 mA h (g-carbon)$^{-1}$ (Region A in Fig. 1). Most commercial lithium-ion cells employ carbonaceous materials of this region at present. With decreasing HTT from 2400 °C, the specific capacity decreases, reaches the minimum at HTT=1800—2000 °C, and then increases again (Region B in Fig. 1). It has been reported that soft carbons heat-treated at temperatures below 1000 °C have extremely high specific capacities in the range 500—1000 mA h g^{-1} (Region C in Fig. 1). On the other hand, while hard carbons have been already used in some commercial lithium-ion cells, they generally have specific capacities lower than those of soft carbons. However, recently they have attracted much attention, since it was shown that some kinds of hard carbons heat-treated at ca. 1000 °C have high specific capacities in the range 500—700 mA h g^{-1} (Region D in Fig. 1). These four categories of carbon have been used in commercial lithium cells or are promising candidates in the near future. Their charge and discharge characteristics and intercalation mechanisms are described in the following sections.

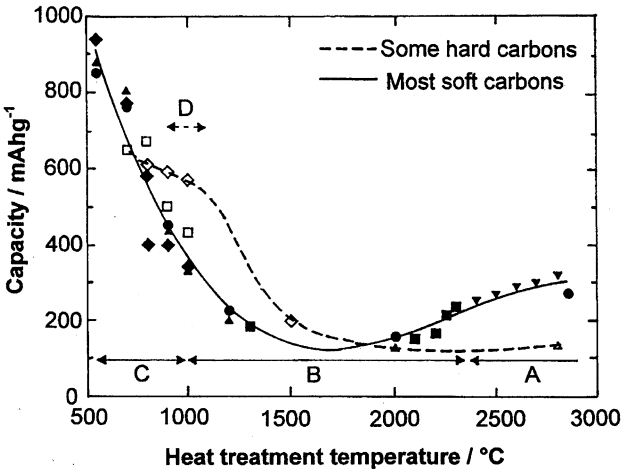

Fig. 1. Relationships between reversible specific capacity and HTT.[5] Closed and open circles shows data obtained for soft and hard carbons, respectively. Regions A—D correspond to those used in the text.

(a) Graphite (Region A). Graphite and soft carbons heat-treated above 2400 °C belong to Region A. Figure 2 shows typical charge and discharge characteristics of a natural graphite powder anode (NG-7, Kansai Coke and Chemicals Co., Ltd.). At the first charging (intercalation), the potential drops rapidly after subtle retardation at ca. 0.8 V. The main intercalation and deintercalation of lithium take place at potentials <0.25 V vs. Li/Li$^+$, associated with some potential plateaus. The charge consumed by the first charging (ca. 400 mA h g^{-1}) is not fully recovered by the following discharging (ca. 320 mA h g^{-1}). The capacity that cannot

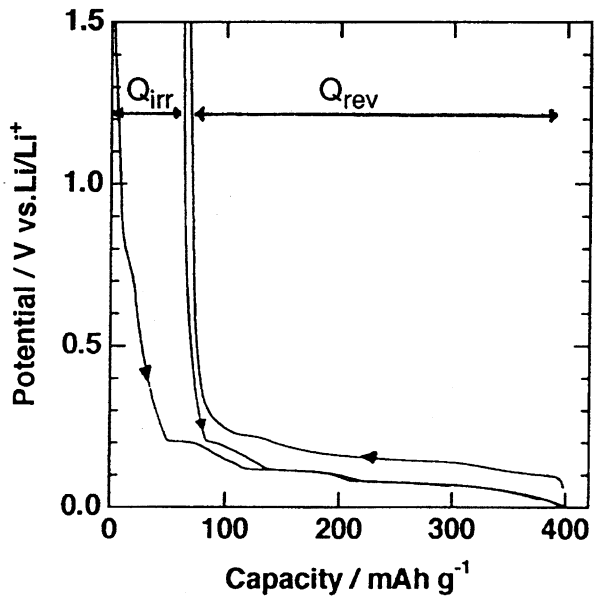

Fig. 2. Charge and discharge characteristics of natural graphite powder (NG-40, Region A) at the first charge-discharge cycle and the following charging in 1 M $LiClO_4$/ethylene carbonate (EC)+diethyl carbonate (DEC) (1 : 1 by volume).

be recovered is called "irreversible capacity" (Q_{irr}), which is more or less observed at the first charge–discharge cycle of any carbonaceous materials. At the second and subsequent cycles, graphite shows good reversibility (rechargeability). The reversible specific capacity (Q_{rev}) typically ranges from 300 to 370 mA h g^{-1}.

Lithium is intercalated within graphite to form graphite intercalation compounds (GICs).[6—8] GICs are layered compounds, in which atomic or molecular layers of a different chemical species called the intercalate, are inserted between graphene layers of host graphite.[9] The most important and characteristic property of GICs is the staging phenomenon, which is characterized by intercalate layers that are periodically arranged in a matrix of graphene layers. Schematic illustrations for staged structures of GICs are shown in Fig. 3a. These staged structures are designated in terms of stage index n, which denotes the number of graphene layers between adjacent intercalate layers, as shown in Fig. 3a. It has been known that lithium can be intercalated within graphite to form Li-GIC since the discovery by Herold[10] in 1955. The phase diagram of Li-GIC, which was obtained by a vapor-phase process, is shown in Fig. 4.[11] Four different staged structures of Li-GICs (n=1—4) are known depending on the concentration of lithium. Here, shaded zone correspond to the mixture of stages. It should be noted that each single-phase region is restricted in a narrow concentration range at room temperature and thereby two different phases coexist throughout almost the whole concentration range. Electrochemical intercalation of Li into graphite has been known to

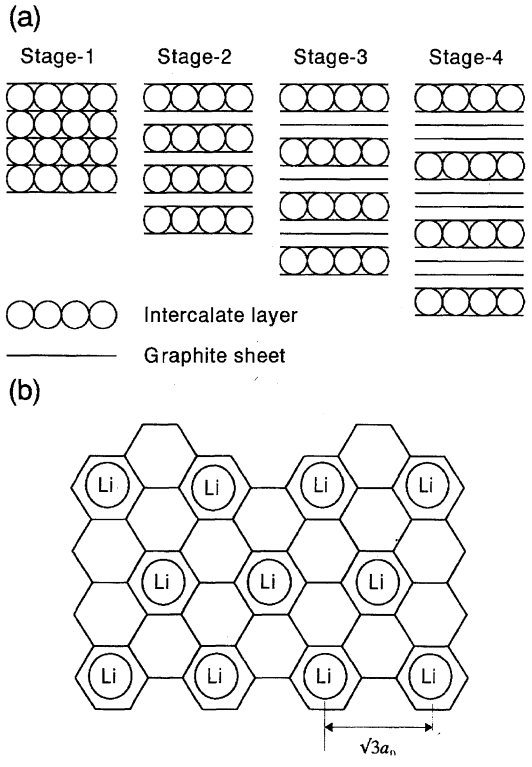

Fig. 3. (a) Stage structures of GICs and (b) in-plane structure of stage-1 Li-GIC.

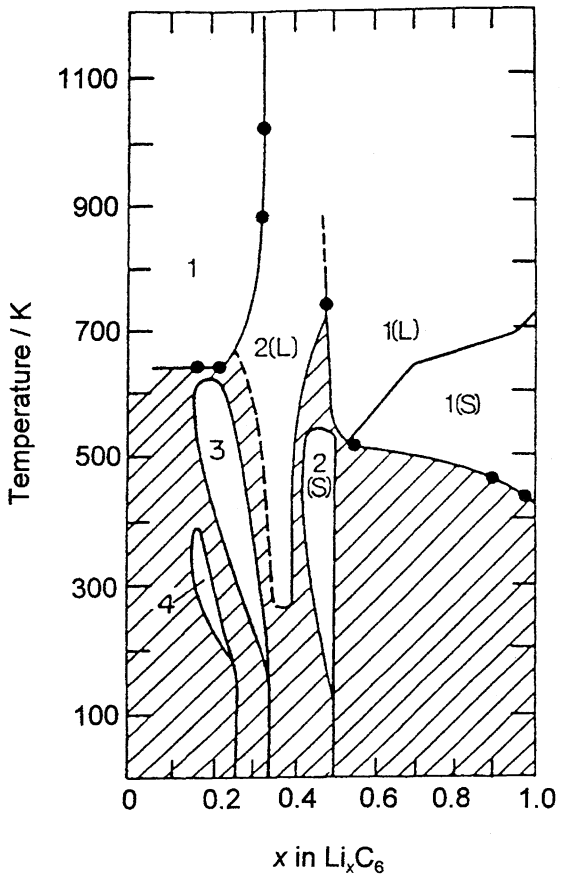

Fig. 4. Phase diagram of Li-GIC prepared by a vapor-phase reaction. The numbers in the diagram show the stage indices. Symbols S and L mean that the intercalate layers are in solid and liquid states, respectively.[11] 1 denotes a dilute stage 1, and 3 and 4 correspond to dense stage 3 and 4, respectively.

give the same staged structure of Li-GICs.[6] Similar to the vapor-phase process, each single-phase region is restricted. The detail is given later. Another important feature of GICs is the in-plane ordering of the intercalate with respect to the adjacent graphite layers called "superlattice structure". The superlattice structure of stage-1 Li-GIC is shown in Fig. 3b,[12] in which lithium exhibits a $\sqrt{3}\times\sqrt{3}$ structure. The composition of stage-1 Li-GIC thus resulted in LiC_6.

The mechanism of lithium intercalation within graphite has been studied so far using X-ray diffraction (XRD).[6—8] Each electrochemical reaction takes place at the interface between an electrode and an electrolyte solution. Hence, it is very important to know the phenomena taking place at the interface as well as bulk structural changes and diffusion within the bulk. Laser Raman spectroscopy gives information about phenomena within an optical skin depth for the incident laser beam. In the case of carbonaceous materials, the depth is of the order of 100 nm for light scattering at 514.5 nm,[13] and very convenient to study the phenomena taking place just at the interface. Accordingly, the authors have employed an in situ Raman technique to clarify the intercalation and deintercalation processes during charging

and discharging.

Hexagonal graphite crystallizes in the $P6_3/mmc$ space group, and has four carbon atoms in its unit cell. By factor group analysis, the irreducible representation of the optical modes (Γ) is shown as:[14]

$$\Gamma = A_{2u} + 2B_{1g} + E_{1u} + 2E_{2g} \,. \quad (2)$$

Of these, two doubly degenerate E_{2g} modes are Raman active. Pristine graphite exhibits two Raman modes at 42 and 1580 cm^{-1}, which are designated as E_{2g1} and E_{2g2}, respectively. Figure 5 shows in situ Raman spectra of the edge plane of highly oriented pyrolytic graphite (HOPG) obtained during charging (lithium intercalation).[15] The 1580 cm^{-1} band before charging (3.11 V) in Fig. 5a shows the Raman-active E_{2g2} mode of pristine graphite. The observed changes of this band in Fig. 5 clearly show that lithium is intercalated through formation of GICs. For example, at ca. 200 mV in Fig. 5b the original single peak at ca. 1580 cm^{-1} broadened, and new two lines grew at both sides of the original line. The Raman spectra for GICs with stage $n \geq 3$ are known to exhibit a doublet structure at frequencies close to the original E_{2g2} of pristine graphite.[16] The lower and upper frequency components are assigned to carbon-atom vibrations in "interior graphene layers" (not adjacent to intercalate layer planes) and in "bounding graphene layers" (adjacent to intercalate layer planes), respectively. From their intensity ratio, the

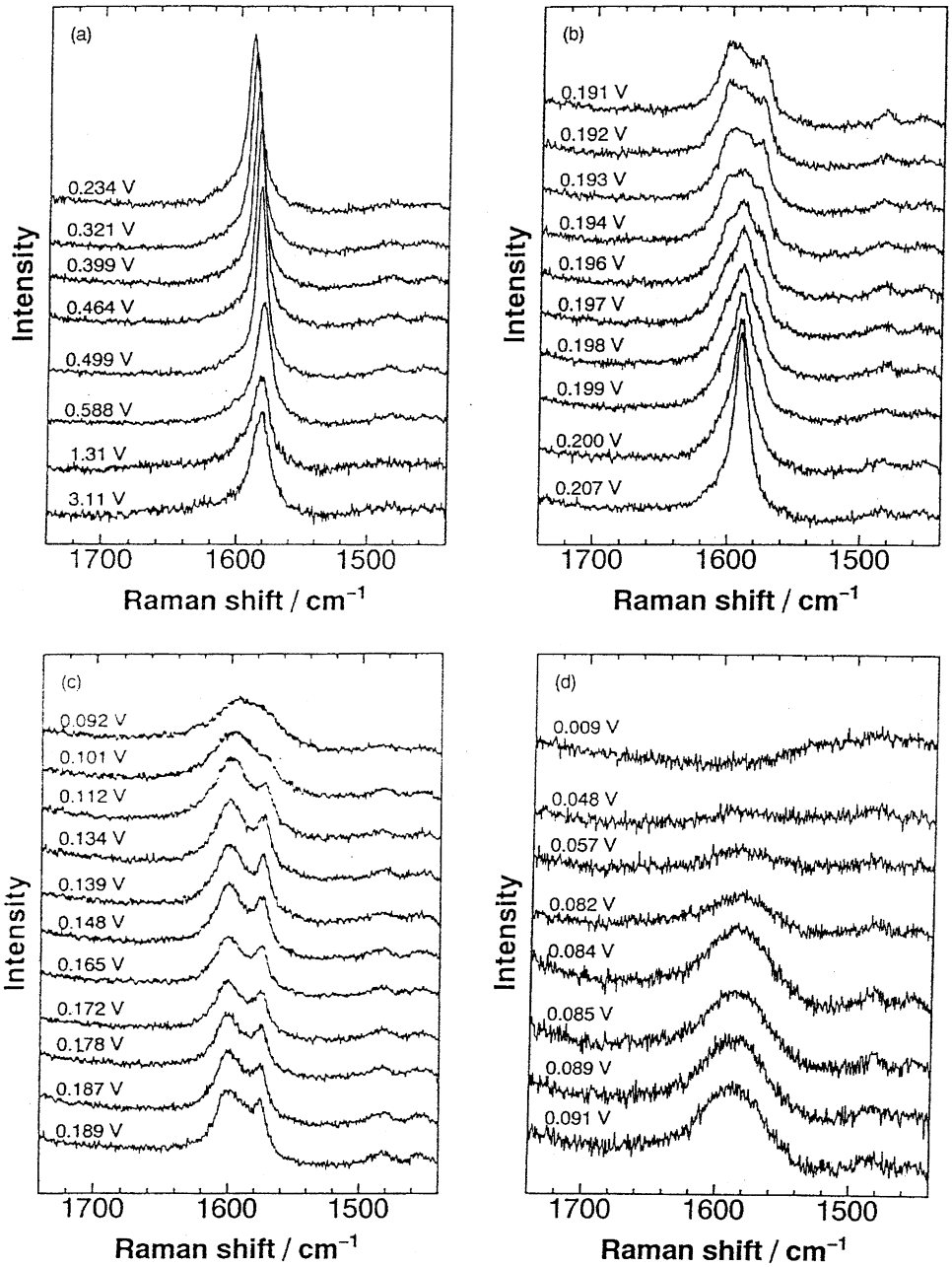

Fig. 5. Variation of in situ Raman spectra of HOPG (3.1 mg) edge plane with various potentials (a) from 3.11 to 0.234 V, (b) from 0.207 to 0.191 V, (c) from 0.189 to 0.092 V, and (d) from 0.091 to 0.009 V upon lithium intercalation in 1 M $LiClO_4$ EC/DEC.[15]

new two lines are assigned to the doublet of stage-4,[17] which means that a stage transition from dilute stage-1 to stage-4 took place at this potential. Here dilute stage-1 denotes a phase in which lithium is intercalated uniformly within the host.[18] For further detailed changes of spectra in Fig. 5, readers are refereed to original paper[15] and review articles.[19] From these Raman spectral changes, it was shown that the following stage transitions take place upon electrochemical lithium intercalation and deintercalation:

Dilute stage-1	↔	Stage-4	(ca. 210 mV)
Stage-2L	↔	Stage-2	(ca. 120 mV)
Stage-2	↔	Stage-1	(ca. 90 mV)

where stage-2L denotes a liquid-like stage-2 phase that has no in-plane ordering. As shown by the phase diagram in Fig. 4, two different phases coexist over almost the whole composition range except in limited single-phase regions. In such two-phase coexistence regions, the electrode potential is thermodynamically fixed at a single potential, which results in the observed potential plateaus in charge and discharge profiles. These results are in good agreement with those obtained from XRD studies using graphite powder electrodes,[6–8] but it should be noted again that the Raman spectra give information about processes taking place just at the electrode/electrolyte interface. Since an HOPG block was used in the above Raman measurements, lithium would not have been fully intercalated into the interior of the block within the time scale of the charge-discharge test. Nevertheless, the results are in agreement with those obtained from XRD studies using powder electrodes. This implies that the GIC structure at the surface adjacent to the solution determines the electrochemical properties, such as potential, of the intercalation reaction.[15]

As shown earlier, graphite allows lithium intercalation up to a composition of LiC_6. This restricts the specific capacity of graphite to 372 mA h g^{-1}. Because of the low and flat discharge profile and high reversibility of the reaction, highly graphitized carbons have been already used as anode materials in commercial lithium-ion cells.

(b) Soft Carbons Heat-Treated in the Range 1000—2400 °C (Region B). Graphitized soft carbons in Region A have reversible capacities over 300 mA h g^{-1}. With decreasing HTT below 2400 °C (Region B), the reversible capacity decreases, reaches a minimum at ca. 2000 °C, and then increases again. Figure 6 shows the variation of charge-discharge characteristics of a petroleum pitch-based soft carbon with HTT.[20] HTT affects not only the reversible capacity, but also the shape of charge and discharge curves. Soft carbons heat-treated at temperatures below 2000 °C do not show any potential plateaus on charge and discharge profiles, and the potential changed monotonously. Figure 7 shows the variation of Raman E_{2g2} band of a spherical mesophase pitch-based carbon (mesocarbon microbeads; MCMBs; HTT= 1800 °C) during charging and discharging.[21] With a drop in potential by charging (Fig. 7a), the E_{2g2} band shifted downward, and its intensity decreased. On the contrary, upon discharging the E_{2g2} band shifted in the opposite direction (Fig. 7b). Lithium insertion raises the electron density on carbon layers, while lithium species inserted between the carbon layers were charged positively.[22] In donor-type GICs, the charge is transferred into an antibonding π band of graphite.[22] This weakens the intralayer C–C bonds, and the E_{2g2} band is expected to shift downward upon charging and upward upon discharging. Hence, the observed spectral changes indicate that lithium was inserted between carbon

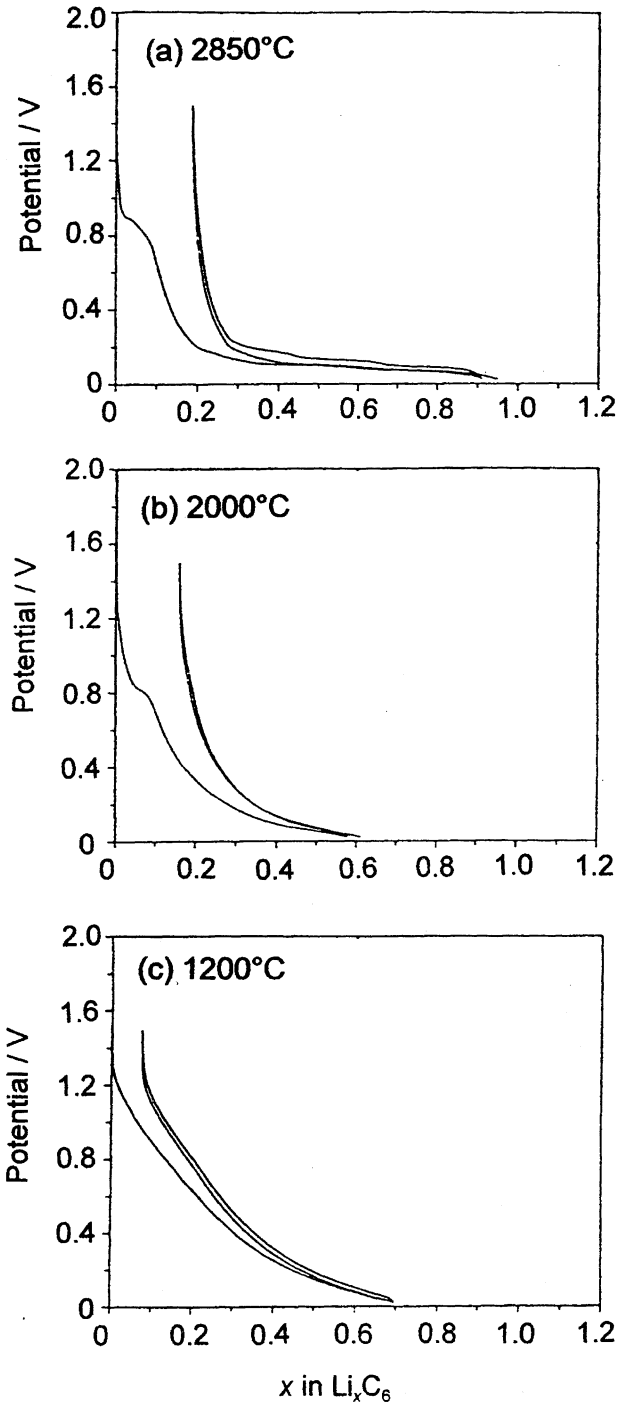

Fig. 6. Variation of charge-discharge characteristics of petroleum pitch-based soft carbons heat-treated at (a) 2850, (b) 2000, and (c) 1200 °C in 1 M $LiN(CF_3SO_2)_2$+1 M 12-crown-4/Propylene carbonate (PC)+EC (1 : 1 by volume).[20]

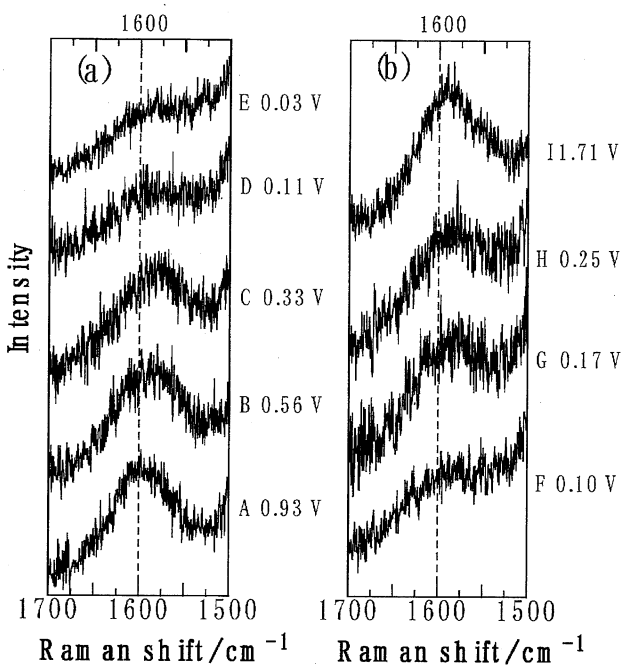

Fig. 7. In situ Raman spectra of MCMBs (HTT=1800 °C, Region B) at various potentials upon (a) charging and (b) discharging in 1 M $LiClO_4$/EC/DEC (1 : 1).[21]

layers of MCMB (HTT=1800 °C). However, this downward-shift of the E_{2g2} band was continuous, and no change indicative of staged phase formation was observed. These facts show that lithium is inserted randomly between carbon layers of MCMB (HTT=1800 °C) without the formation of any staged structures.[21]

Soft carbons in this region contain many imperfections, such as turbostratic disorder and unorganized parts in their crystallites. Dahn et al. reported that the maximum reversible capacity (x_{max}) in this region can be well described by the following expression:

$$x_{max} = g\{(1-P)1 + Px_r\} + (1-g)x_u , \quad (3)$$

where g, P, x_r, and x_u denote the fraction of low strain part, the probability of finding turbostratic disorder, the reversible capacity of unstrained carbon layers with turbostratic disorder (random shifts or rotations), and that of highly strained unorganized carbon, respectively. For soft carbons, calculated reversible capacities are in good agreement with experimental ones when x_r=0.3 and x_u=0.9 are assumed.[20] When lithium is intercalated into graphite between adjacent parallel graphene layers, these layers shift from ABAB··· into AAAA··· stacking.[23] Therefore, carbon layers with turbostratic disorder will most likely be pinned and hence be unable to shift into the AAAA··· stacking arrangement, resulting in a lower capacity (x_r=0.3). On the other hand, the presence of unorganized carbon leads to lower density and gives more space for lithium to be accommodated. This results in a relatively high capacity of the unorganized carbon (x_u=0.9). The unorganized part disappears by heat-treatment up to 2000 °C, while turbostratic disorder is gradually removed by heat treatment at temperatures above 2000 °C; hence, the reversible capacity shows the minimum at HTT of ca. 2000 °C. Tatsumi et al.[24] obtained a similar relationship between the reversible capacity and the probability of finding an ordered stacking sequence (the P_1 parameter[25]).

(c) Disordered Carbons (Regions C and D). It has been recently reported that two categories of disordered carbons have much higher capacities than the theoretical capacity of graphite. One is soft carbons heat-treated below 1000 °C (Region C in Fig. 1),[20,27—33] and the other is hard carbon heat-treated at temperatures in a limited range around 1000 °C (Region D in Fig. 1).[34—40] Both carbons are very promising materials and have attracted much attention of many researchers for use as anodes in high-capacity lithium-ion cells in the near future.

Figure 8 shows charge and discharge characteristics of MCMBs heat-treated at 700 °C, which are typical of carbons in Region C. Although a high irreversible capacity (600 mA h g^{-1}) appeared in the first cycle, a reversible specific capacity of 750 mA h g^{-1} was attained in the subsequent cycles, the capacity of which is twice as high as the theoretical capacity of graphite (372 mA h g^{-1}). One of the characteristic features of Region C carbons is the hysteresis of their charge and discharge profiles; that is, lithium is intercalated near 0 V, but deintercalated at about 1 V as shown in Fig. 8. It was reported that some hard carbons heat-treated below 1000 °C showed similar behavior.[26] Although Region C carbons show high reversible capacities, their low density (ca. 1.5 g cm^{-3}), low coulombic efficiency (50—60%) at the first cycle, and poor rechargeability remained to be solved before use in practical cells. In addition, the hysteresis of the potential profile is one of the disadvantages of Region C carbons because it causes a substantial energy loss.

Since their reversible capacity values are much higher than the theoretical capacity of graphite, the insertion mechanism cannot be explained by the simple model that lithium is inserted between carbon layers. Various models for high capacity carbons in Region C have been suggested so far. Sato et al.[27] analyzed their pyrolyzed poly(*p*-phenylene) using ^{7}Li NMR. Their carbon had a high capacity of 680 mA h g^{-1},

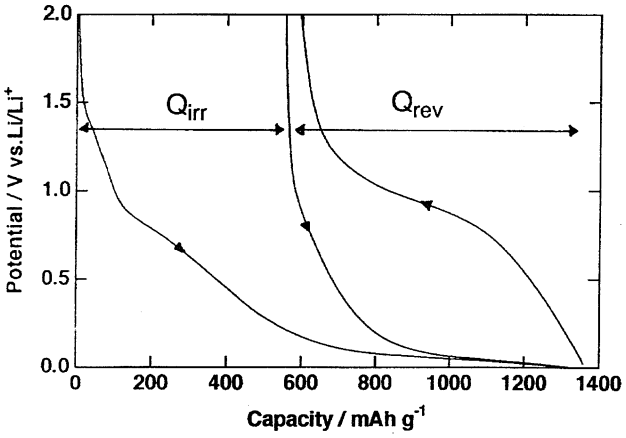

Fig. 8. Charge and discharge characteristics of MCMBs (HTT=700 °C, Region C) at the first charge-discharge cycle and the second charging in 1 M $LiClO_4$/EC+DEC (1 : 1).

and showed two different NMR peaks when lithium was inserted. They assigned the two peaks to ionic Li species and covalent Li_2 molecules, and suggested a mechanism where lithium is inserted between carbon layers with an in-plane LiC_2 structure as shown in Fig. 9. Yata et al.[28] proposed similar in-plane lithium ordering for their polyacenic semiconductors (PAS), but they thought that all lithium species are in an ionic state. Mabuchi et al.[29] studied the charge and discharge characteristics of MCMBs heat-treated at temperatures below 1000 °C. They found that a good correlation between the reversible capacity and the total cavity amount in carbon per unit volume (cavity index). From this fact, they proposed that the high reversible capacity of MCMBs heat-treated below 1000 °C originates from the doping of lithium within nanoscopic cavities in carbon as shown in Fig. 10. Carbons heat-treated below 1000 °C contain significant amounts of residual hydrogen atoms. Zheng et al.[30] showed that the reversible capacity increases proportionally with the H/C ratio of carbon, and suggested a mechanism that the residual H-atoms participate in lithium doping reactions. Recently, they[31] and Zhou et al.[32] proposed a model

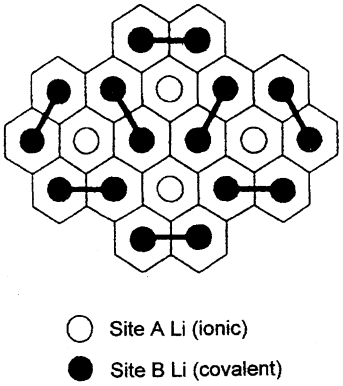

Fig. 9. Schematic illustration for the coexistence of two types of lithium sites in pyrolyzed poly(*p*-phenylene).[27]

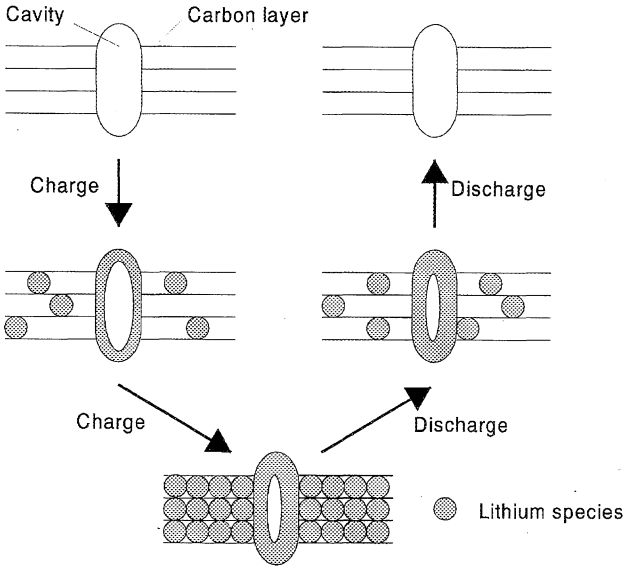

Fig. 10. Cavity model for the charge-discharge processes of MCMBs heat-treated at temperature below 1000 °C.[29]

that lithium atoms bind on the hydrogen-terminated edges of hexagonal carbon fragments.

The authors studied the doping reaction of MCMBs (HTT = 700 °C) using Raman spectroscopy.[21] Panels (a) and (b) in Fig. 11 show the variations of the Raman spectra during charging and discharging, respectively. While the intensity of the E_{2g2} band slightly decreased below 100 mV upon charging [Fig. 11a], the peak frequency did not shift at all in the whole potential range. Moreover, no charge of the E_{2g2} band during discharging was observed in particular in the plateau region at about 1 V [Fig. 11b]. The E_{2g2} band is one of the Raman active lattice vibrations of graphite as mentioned earlier. If lithium was inserted between organized carbon layers, inserted lithium would affect the electronic structure of the organized layers, and thereby the peak frequency of the E_{2g2} band should change. However, no change in peak frequency was observed during charging and discharging. This means that the lithium insertion mechanism of carbons in Region C is different from that of soft carbons heat-treated above 1000 °C, where lithium is inserted between organized carbon layers. Although it is not clear which mechanism most precisely describes the lithium insertion within carbons in Region C, our Raman results suggested that the high capacity does not originate from lithium species inserted between organized carbon layers, and thereby is not consistent with models that lithium is inserted between carbon layers with a high density. It should be noted, furthermore, that the model should explain the large hysteresis of the charge and discharge profiles as well. The presence of hysteresis implies

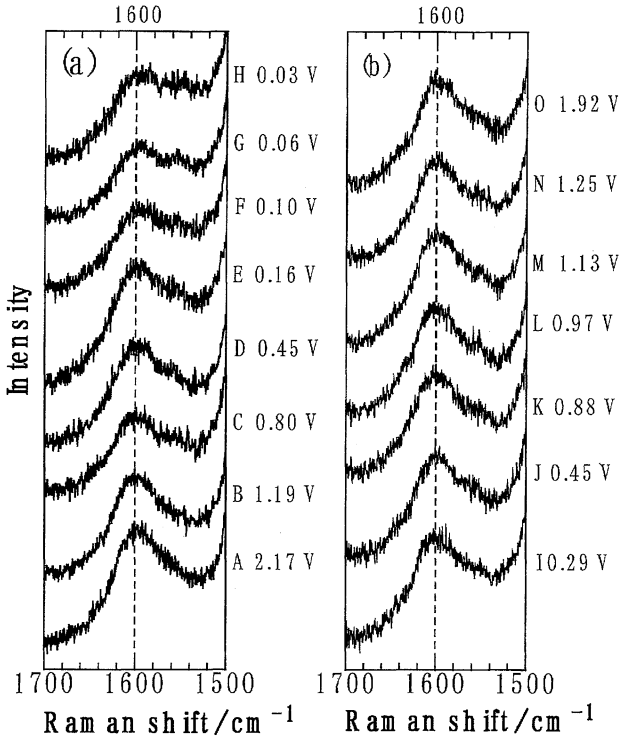

Fig. 11. In situ Raman spectra of MCMBs (HTT=700 °C, Region C) at various potentials upon (a) charging and (b) discharging in 1 M $LiClO_4$–EC/DEC (1 : 1).[21]

that the reaction is not a simple insertion shown by Eq. 1, but a complicated process which involves a kind of following chemical reactions associated with large activation energies, as pointed out by Zheng et al.[33] Further study is necessary to clarify the doping mechanism of this kind of carbon.

Some hard carbons heat-treated at temperatures around 1000 °C also have extremely high reversible capacities in the range 500—700 mA h g^{-1} (Region D in Fig. 1). A typical charge-discharge profile is shown in Fig. 12,[34] which was obtained for petroleum-pitch-based pseudo-isotropic carbon (PIC). Most of lithium insertion and removal take place at potentials below 0.1 V, and the profile showed no hysteresis. In addition, the irreversible capacity in the first cycle is not so high as that of Region C soft carbons. Hard carbons pyrolyzed from petroleum pitch,[35] poly(furfuryl alcohol),[36] and phenolic resins[37] belong to this category. In addition, it was reported that pyrolyzed carbons from natural carbohydrates such as sugar, starch, and wood show similar behavior.[38]

The reversible capacity of these hard carbons is also much higher than that of the theoretical capacity of graphite. However, the voltage profile is quite different from that of the soft carbons, which implies that the mechanism for lithium doping is also different. Ishikawa et al.[39] proposed that such a high capacity corresponds to the filling of micropores in the carbon with a kind of lithium clusters. Liu et al.[40] showed that these carbon materials consist primarily of small single layers of carbon like a "house of cards", and proposed that lithium could be adsorbed on both of the surfaces of these single layers, which leads to a higher capacity than that of graphite.

For practical use as anode of lithium ion batteries, however, the discharge potential of region C carbon (approaching

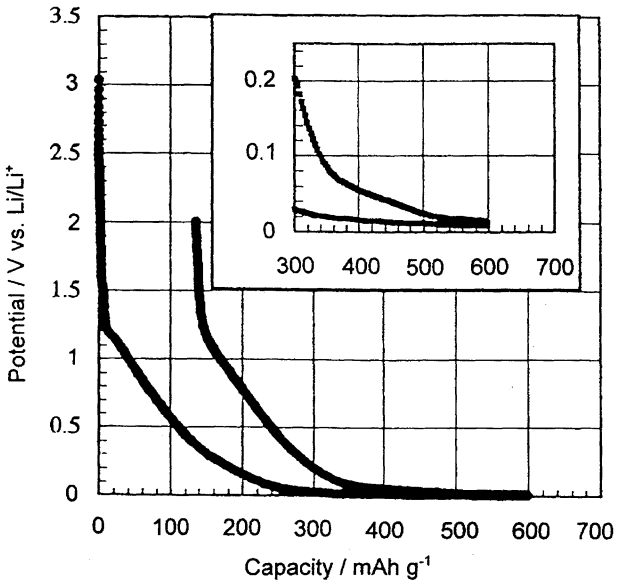

Fig. 12. Charge and discharge characteristics of petroleum-pitch-based pseudo-isotropic carbon (PIC, Region D) at the first cycle in 1 M $LiClO_4$/EC+1,2-dimethoxyethane (DME) (1 : 1).[34]

1 V vs. Li/Li^+ i.e., large hysteresis), charge potential (close to 0 V vs. Li/Li^+ which may cause lithium metal deposition) region D carbon and the low density of both carbon materials are meeting some difficulties; low energy density due to low discharge voltage for C and due to low density for both C and D, and difficult control of charging (dendritic lithium deposition) for D. Some breakthrough such as invention of redox shuttle to suppress dendritic lithium deposition during charging at potential close to 0 V vs. Li/Li^+ would lead to practical use of region D carbon.

Solvent Decomposition and Surface Film Formation on Carbon Anodes

High stability against reduction is one of the required conditions for solvents in lithium-ion cells, because lithium intercalation takes place at extremely negative potentials. Aqueous solutions cannot be used for this reason; instead, aprotic nonaqueous solutions containing lithium salts, such as $LiClO_4$, $LiPF_6$, and $LiBF_4$, as electrolytes are used in lithium-ion cells. 4-methyl-1,3-dioxolan-2-one (propylene carbonate, PC) has high stability against reduction as well as a high dielectric constant, and hence PC or PC-based mixed solvent systems have been employed as a solvent in primary lithium cells using metallic lithium as the anodes. However, this is not the case for lithium-ion cells using carbonaceous materials, in particular graphitized ones, as the anodes. When a graphitized carbon anode is charged in a PC-based electrolyte solution, the solution keeps decomposing at about 1.0 V vs. Li/Li^+, accompanied by the exfoliation of the graphite layers.[41] This problem has been overcome by use of 1.3-dioxolan-2-one (ethylene carbonate, EC)-based mixed solvents.[42] In contrast, such solvent decomposition is not observed when disordered carbons heat-treated below 2000 °C are charged even in PC-based solutions. Furthermore, it was reported that addition of 12-crown-4, which selectively coordinates lithium ion, to PC-based solutions suppresses solvent decomposition, and enables lithium to be intercalated within graphitized carbons.[43] These facts reveal that the ease of solvent decomposition on carbon anodes is not determined solely by the stability of the solvent. Quite recently, Nagayama et al.[44] reported that lithium can be intercalated within graphite in partially fluorinated propylene carbonate (4-trifluoromethyl-1,3-dioxolan-2-one, TFPC). TFPC should be less stable against reduction than PC because it has three fluorine atoms that are strongly electron-withdrawing. This fact clearly shows that some factors other than the stability against reduction dominate the solvent decomposition.

Thermodynamically almost all kinds of organic solvents should be unstable at potentials where lithium is intercalated. It is generally accepted that in EC-based solutions stable surface film is formed on carbon anodes at ca. 1 V upon the first charging and thereby the carbon surface is passivated. The film is called "solid electrolyte interface" (SEI) by Peled.[45] It has lithium-ion conductivity, but does not show electronic conductivity. Hence the film suppresses further solvent decomposition, but through this film lithium ion can be in-

tercalated within carbons. It is widely recognized that SEI formation is one of the origins of the irreversible capacity. The irreversible capacity increases with an increase in the surface area of carbon.[46]

Aurbach et al.[47] analyzed the composition of the surface film on carbon anodes by in situ FT-IR, and reported that reduced products of solvent, such as $ROCO_2Li$ for alkyl carbonate-based solvent react with water or CO_2 dissolved in the system to form a layer of Li_2CO_3, which functions as SEI on graphite. Similar reaction schemes were proposed by Shu et al.[43] Takai et al.[48] reported that the thickness of SEI formed on carbon black was ca. 1—1.5 nm, which is much thinner than similar kind of SEI formed on metallic lithium electrode (ca. 100 nm). Besenhard et al.[49] studied the crystal expansion of HOPG during electrochemical reduction in an EC-based solution by dilatometry, and observed a drastic expansion of the graphite matrix (>150%) at potentials more negative than 1.0 V vs. Li/Li^+. They attributed this expansion to solvent co-intercalation, and concluded that the intercalated solvent further decomposes to form an immobile product which remains between the graphene layers and that this reduction product prevents further solvent intercalation and the exfoliation of graphite layers.

The authors have employed electrochemical scanning tunneling microscopy (STM) to clarify the mechanism of surface film formation on carbon anodes.[50,51] Electrochemical STM is a powerful new technique for detailed structural and topographical characterization of electrode/electrolyte interfaces.[52] Knowledge of surface structures could be crucial to the understanding of surface film formation that is taking place at the electrode surface. As the test carbon material, HOPG was selected because an atomically flat basal plane can be obtained easily by cleaving the surface layers with a piece of adhesive tape.

A typical STM image of HOPG basal plane is shown in Fig. 13a, which was obtained at 2.8 V obtained in a 1 M

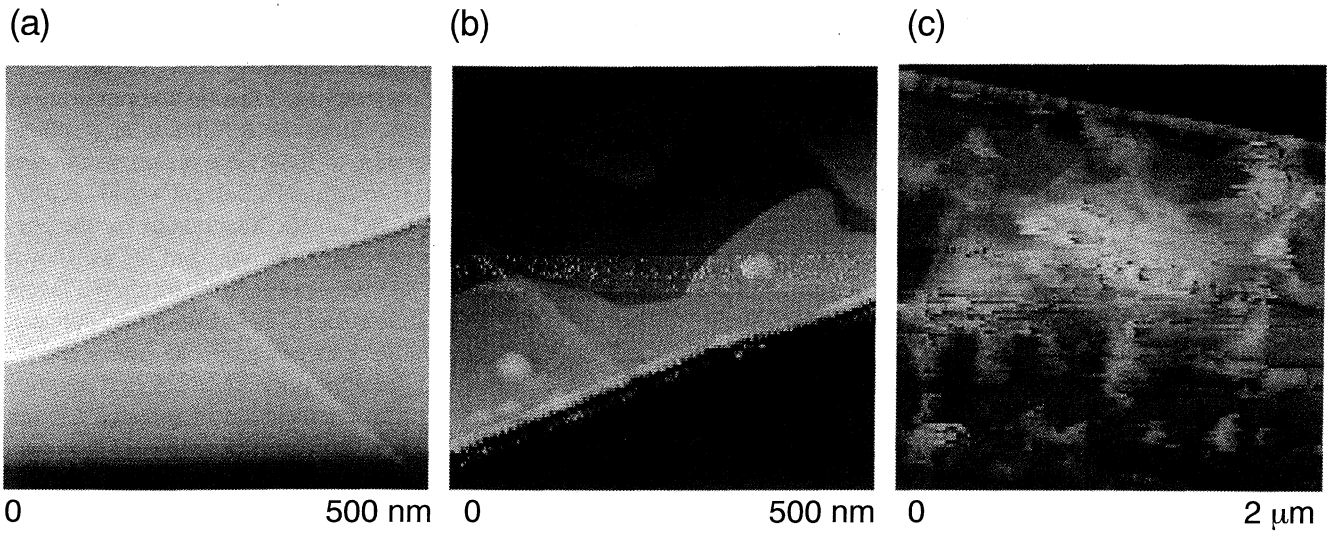

Fig. 13. Electrochemical STM images of HOPG basal plane at (a) 2.8, (b) 1.1 V, and (c) after potential was stepped to 0.75 V for 1 min in 1 M $LiClO_4$/EC+DEC (1 :1).[50,51] Images (a) and (b) are of nearly the same position, but image (c) shows different part.

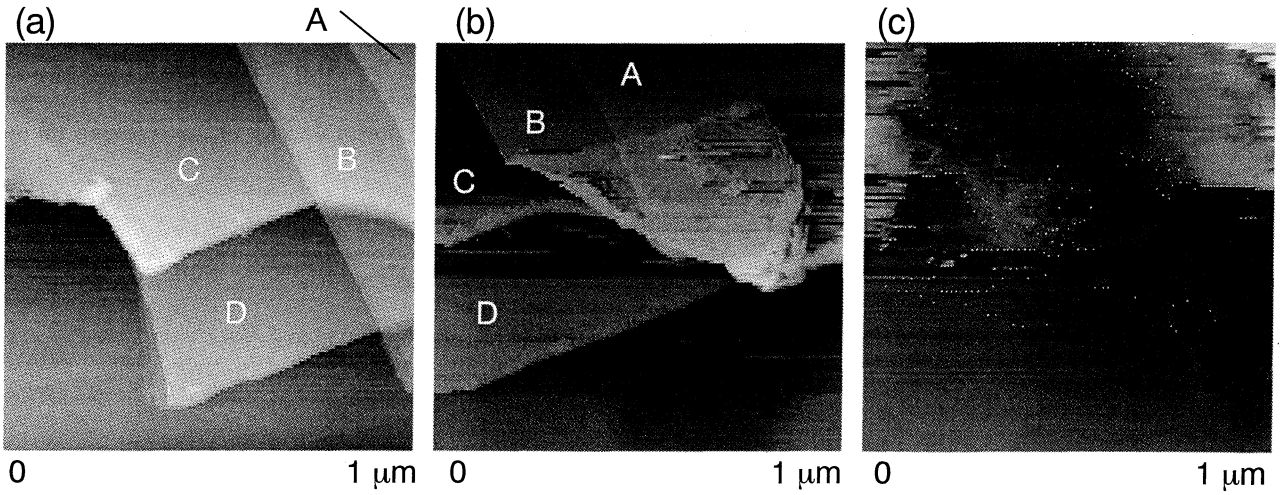

Fig. 14. Electrochemical STM images of HOPG basal plane after the potential was stepped to (a) 1.1 V, (b) 0.95, and (c) 0.7 V for 30 s in 1 M $LiClO_4$/PC.[51]

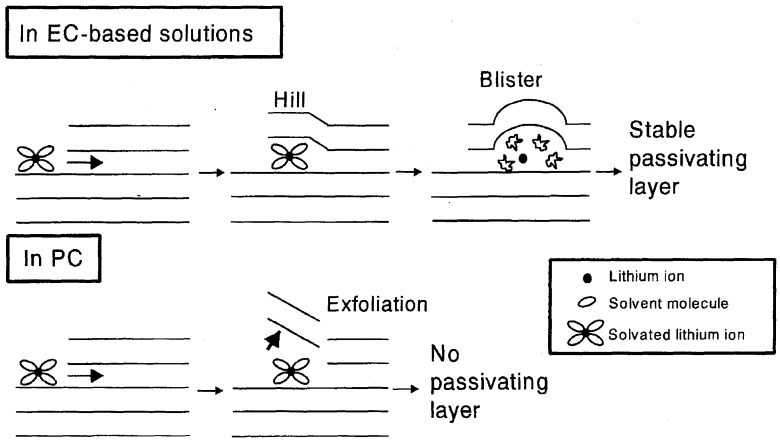

Fig. 15. Schematic illustrations explaining the morphology changes in EC-based solutions and PC.

solution of $LiClO_4$ (1 M=1 mol dm^{-3}) in a mixture of EC and diethyl carbonate (DEC) (1 : 1 by volume). A clear step of 3-nm height was seen horizontally in the image. When the potential was stepped to 1.1 V (Fig. 13b), two "hill-like" features appeared at the upper part of the image and in the vicinity of the step edge. The height of both hills was 0.8—1 nm, and the hilltop was atomically flat. The shape of the latter hill at the step edge clearly shows that it was formed from the step edge and then spread out. An atomic scale STM image of the hilltop showed every other atom on the hexagonal carbon network of the graphene layer as bright spots spaced by ca. 0.25 nm on a 2-dimensional triangular lattice, which is a typical STM image of graphite basal plane.[53] This fact indicates that the top surface consisted of graphene layers of ABAB··· stacking, and thereby the hill was an interior structure formed beneath the surface.[51] The observed height of the hill-like structure, ca. 1 nm, is comparable to the interlayer spacings of stage-1 ternary GICs of alkali metal with organic molecules, such as tetrahydrofuran and 1,2-dimethoxyethane, prepared by a solution method.[54] It was thus concluded that solvated lithium ion is intercalated between graphene layers at this potential to form the hill-like structures, which supports the solvent-cointercalation model proposed by Basenhard et al. After the potential was kept at 0.75 V, a significant change in surface morphology was observed as shown in Fig. 13c.[51] Large blisters in irregular shapes were formed on the surface. The maximum height of the blisters was ca. 20 nm, which was much higher than that of the hills (ca. 1 nm). These blisters seem to have been formed by accumulation of decomposition products of the solvated lithium ion and by rupturing of the graphene layers.

In contrast, morphology changes in a 1 M solution of $LiClO_4$ dissolved in PC were quite different as shown in Fig. 14. Hill-like structures or blisters were not formed in 1 M $LiClO_4$/PC, but only rapid exfoliation and rupturing of graphite layers occurred. Since the exfoliation of graphene layers leads to regeneration of fresh edge planes, stable surface film would not be formed and PC solvent would keep decomposing ceaselessly. Schematic illustrations for the phenomena occurring in EC-based solutions and PC are shown in Fig. 15. It is not clear why exfoliation of graphite layers occurs in only PC solution. In EC-based solutions, solvated Li^+ ion can stay securely between graphene layers and be subject to subsequent decomposition, resulting in stable surface film formation. The intercalation of solvated Li^+ ion may therefore be a necessary step for stable surface film formation on carbon anodes.

Lithium Diffusion within Carbonaceous Materials

Lithium intercalation involves lithium diffusion within host carbonaceous materials. Since diffusion in solid is generally a slow process, the diffusion rate would dominate the overall reaction rate, that is, the maximum charge–discharge current. The diffusion coefficient of lithium within carbonaceous materials (D_{Li^+}) is thus a critical parameter that determines the power density of the resulting lithium-

Table 1. Diffusion Coefficients of Lithium Ion (D_{Li^+}) in Various Carbonaceous Materials

Sample	Morphology	Composition (x in Li_xC_6)	D_{Li^+} / cm^2 s^{-1}	Method	Reference
Petroleum coke	Powder	$0 \leq x \leq 0.6$	1.5×10^{-7}—1×10^{-8}	GITT[a]	(55)
Natural graphite	Powder	$0 \leq x \leq 0.6$	1×10^{-6}—1×10^{-9}	AC impedance	(58)
Natural graphite	Powder	$0 \leq x \leq 1$	10^{-7}—10^{-10}	AC impedance	(60)
Pitch-based coke	Fiber	$0 \leq x \leq 0.5$	1×10^{-10}—2×10^{-11}	AC impedance	(59)
Pitch-based coke	Fiber	$0 \leq x \leq 0.6$	2×10^{-10}—4×10^{-13}	CPR,[b] PSCA[c]	(57)
Pitch-based coke	Powder	$0 \leq x \leq 0.4$	3×10^{-8}—1×10^{-9}	CPR,[b] PSCA[c]	(56)

a) Galvanostatic intermittent titration technique. b) Current pulse relaxation. c) Potential step chronoamperometry.

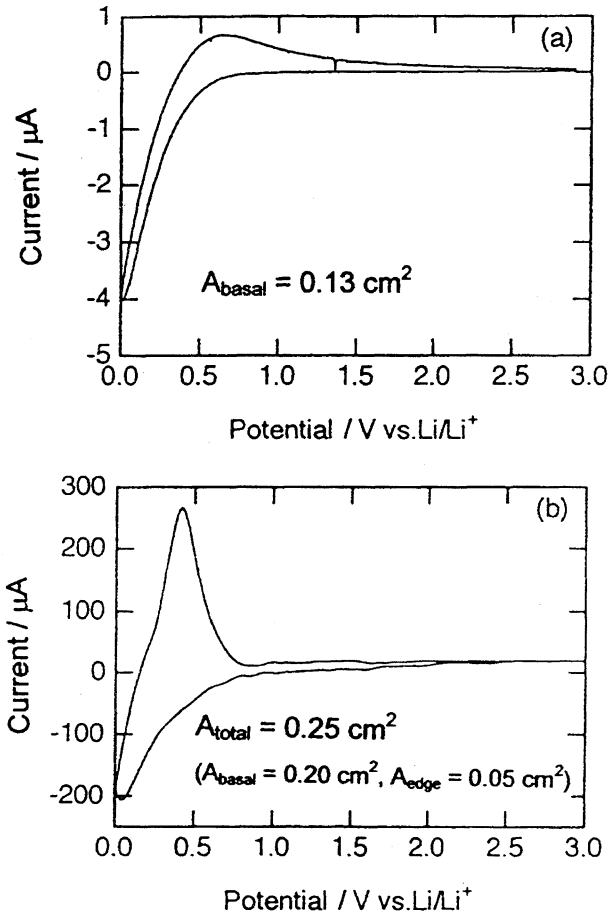

Fig. 16. Cyclic voltammograms at the second cycle of (a) basal plane (0.13 cm^2) of a HOPG block and (b) the whole surface of a HOPG piece (0.25 cm^2) in 1 M $LiClO_4$/EC+DEC (1 : 1).[62] v=0.1 mV s^{-1}.

ion cells. The values of D_{Li^+} have been determined by several methods including galvanostatic intermittent titration technique (GITT),[55] current pulse relaxation (CPR),[56,57] potential step chronoamperometry (PSCA), and AC impedance spectrscopy.[58—60] Some of the data determined by these techniques are summarized in Table 1. The values of D_{Li^+} are rather scattered over a wide range of 10^{-6}—10^{-13} cm^2 s^{-1} depending on the kind of carbon and on the technique employed. To obtain D_{Li^+} by using these methods, one has to know the surface area of the sample, A, and in some cases, the variation of the open-circuit potential with lithium composition, dV_{oc}/dx. However, precise determination of A and dV_{oc}/dx is difficult in general, which is one of the reasons for the scattering of the data.

Carbonaceous materials based on the graphite crystal lattice are highly anisotropic, as mentioned earlier. Such anisotropic structure is also an important factor to determine the diffusion behavior of lithium. Imanishi et al.[61] used carbon fibers of different microtextures (onion-like, radial, and random), and studied the effect on the behavior of lithium intercalation and deintercalation. They reported that the microtexture greatly affects the charge and discharge characteristics such as reversible capacity, although it is not

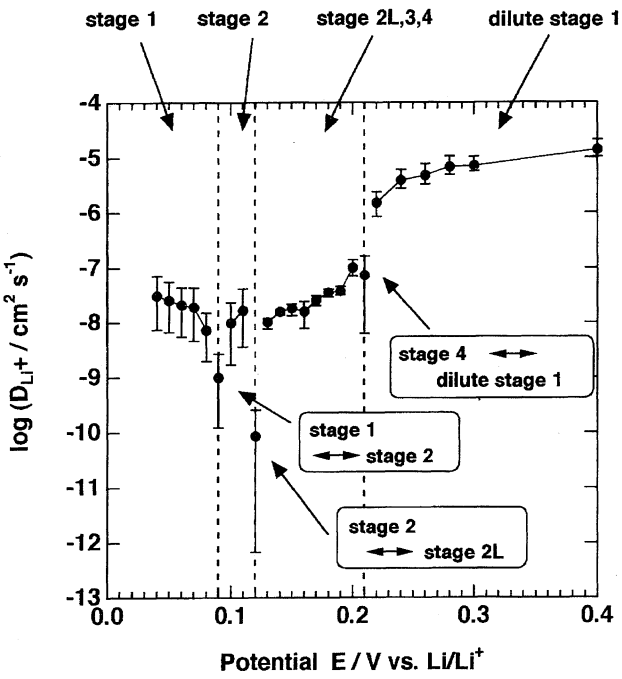

Fig. 17. Chemical diffusion coefficients of lithium within graphite plotted against electrode potential.[60]

the sole factor. The effect of anisotropy of carbon is made clearer by comparison of the two cyclic voltammograms of HOPG in Fig. 16.[62] Curve (a) in Fig. 16 shows the voltammogram when only the basal plane was in contact with the electrolyte solution, whereas curve (b) was obtained when the whole piece of HOPG block was soaked in the solution. In the latter case [curve (b)], the intercalation and deintercalation current were two orders of magnitude larger than that in the former case [curve (a)]. This fact means that lithium intercalation mainly takes place at the edge plane, and then diffuse to the interior in the direction parallel to the basal plane.[62]

In the case of graphite or highly graphitized carbons (Region A in Fig. 1), it should be noted that the intercalation proceeds through formation of staged GICs. Figure 17 shows the variation of D_{Li^+} of natural graphite powder anode with electrode potential, which was obtained by the authors using AC impedance spectroscopy.[60] D_{Li^+} tends to decrease with a drop in electrode potential, that is, with an increase in lithium content, as is generally observed for other carbonaceous materials. Two characteristic features are seen in Fig. 17. One is that D_{Li^+} in staged GICs is one or two orders of magnitude smaller than that in dilute stage-1 phase, which does not have a distinct staged structure. This clearly shows that the ordering of the host and intercalate layers affects the diffusion coefficient of the mobile ion in GICs. The other feature is that D_{Li^+} abruptly drops at 0.21, 0.12, and 0.09 V vs. Li/Li$^+$. As mentioned earlier, stage transitions occur at these potentials; that is, two different phases coexist at these potentials. Under such conditions, D_{Li^+} does not exactly describe the diffusivity of lithium within graphite, because it is a parameter that is defined in a uniform medium. Since the two-phase coexistence regions make major contributions

to the reversible capacity of graphite anode (see Fig. 2), the diffusivity of lithium in the regions is more important for elucidating the performance of graphite anodes. In a two-phase region, phase transition is accompanied by the movement of the phase boundary;[63,64] however, no quantitative analysis of phase boundary movement has been done in the system of Li-GIC. In order to understand the kinetic aspect of the intercalation within graphite in more detail, it is essential to clarify the kinetics of phase boundary movement.

Concluding Remarks

In this review article, the authors focused on three fundamental aspects of electrochemical lithium intercalation: intercalation mechanism, surface film formation, and lithium diffusion, and presented some recent topics including the results of the authors. Although small-size lithium-ion cells have been already commercialized, much higher energy density is expected for carbon anodes with the rapid development of electric devices today. Furthermore, recent global environmental issues demand urgent development of large-scale, high-capacity lithium-ion batteries for use in electric energy storage and electric vehicles. As mentioned in the text, many carbonaceous materials have been studied for use as one of the candidates of carbon anode for lithium ion batteries. Among these materials, graphitized carbons seem to be the best so far when discharge profiles and reversibility are considered. However, the reversible capacity of graphitized carbons, which are most commonly used in commercially available lithium-ion cells, is theoretically limited to 372 $mA\,h\,g^{-1}$ at maximum. Quite recently Kasuh et al.[65] reported that a special kind of graphitized carbon shows a reversible capacity over 400 $mA\,h\,g^{-1}$ although details are unknown. These carbons are promising anode materials for large-scale, high-capacity lithium-ion batteries in the future, although several problems remain to be solved before use in practical batteries.

In addition to a high reversible capacity, a small irreversible capacity and fast lithium diffusion in the host are also required for use in practical batteries as described in the text. These aspects are often ignored despite their importance for practical use, and studies on these aspects have just started. In order to optimize the battery performance, further fundamental study is necessary in addition to the development of high capacity carbons.

Financial support by a Grant-in Aid for Scientific Research from the Ministry of Education, Science, Sports and Culture and the aid of Asahi Glass Foundation, Japan are greatly appreciated.

References

1) J. R. Dahn, A. K. Sleigh, H. Shi, B. M. Way, W. J. Weydanz, J. N. Reimers, Q. Zhong, and U. von Sacken, "Lithium Batteries, New Materials and New Prospectives," ed by G. Pistoia, Elsevier North-Holland, New York (1993), pp. 1—47.

2) Doping of lithium within fullerenes may be possible; however, they are not likely candidates for lithium-ion batteries because of their solubility in nonaqueous solutions and poor electrochemical reversibility.

3) a) L. Seger, L.-Q. Vwn, and J. Schlenoff, *J. Electrochem. Soc.*, **138**, L82 (1991); b) R. Compton, R. Spackman, D. Riley, R. Wellington, J. Eklund, A. Fischer, M. Green, R. Doothwaite, A. Stephens, and J. Turner, *J. Electroanal. Chem.*, **344**, 235 (1993).

4) R. E. Franklin, *Proc. R. Soc. London, Ser. A*, **A209**, 196 (1951).

5) J. R. Dahn, T. Zheng, Y. Liu, and J. S. Xue, *Science*, **270**, 590 (1995).

6) J. R. Dahn, *Phys. Rev.*, **B44**, 9170 (1991).

7) T. Ohzuku, Y. Iwakoshi, and K. Sawai, *J. Electrochem. Soc.*, **140**, 2490 (1993).

8) Z. Jiang, M. Alamair, and K. M. Abraham, *J. Electrochem. Soc.*, **142**, 333 (1995).

9) a) M. S. Dresselhaus and G. Dresselhaus, *Adv. Phys.*, **30**, 139 (1981); b) "Graphite Intercalation Compounds," ed by H. Zabel and S. A. Solin, Springer-Verlag, New York (1992), Vol. 1&2.

10) A. Herold, *Bull. Soc. Chim. Fr.*, **187**, 999 (1955).

11) a) K. C. Woo, H. Mertwoy, J. E. Fisher, W. A. Kamitakahara, and D. S. Robinson, *Phys. Rev., Sect. B*, **B27**, 7831 (1983); b) J. E. Fisher, C. D. Fuerst, and K. C. Woo, *Synth. Met.*, **7**, 1 (1983); c) D. P. DiVincenzo and T. C. Koch, *Phys. Rev., Sect. B*, **B30**, 7092 (1984).

12) "Kokuen Sokan Kagoubutu (Graphite Intercalation Compounds)," ed by Tanso Zairyo Gakkai, Realize, Tokyo (1990), p. 91.

13) S. A. Solin, "Graphite Intercalation Compounds I," ed by H. Zabel and S. A. Solin, Springer-Verlag, Berlin (1990), pp. 157—219.

14) R. J. Nemanich, G. Lucovsky, and S. A. Solin, *Solid State Commun.*, **23**, 117 (1977).

15) M. Inaba, H. Yoshida, Z. Ogumi, T. Abe, Y. Mizutani, and M. Asano, *J. Electrochem. Soc.*, **142**, 20 (1995).

16) a) C. Underhill, S. Y. Leung, G. Dresselhaus, and M. S. Dresselhaus, *Solid State Commun.*, **29**, 769 (1979); b) P. C. Eklund, G. Dresselhaus, M. S. Dresselhaus, and J. E. Fischer, *Phys. Rev., Sect. B*, **B21**, 4705 (1980); c) T. C. Cheiu, G. Timp, M. S. Dresselhaus, M. Endo, and A. W. Moore, *Phys. Rev., Sect. B*, **B27**, 3686 (1983).

17) G. L. Doll, P. C. Eklund, and J. E. Fischer, *Phys. Rev., Sect. B*, **B36**, 4940 (1987).

18) S. A. Safran, *Phys. Rev. Lett.*, **44**, 937 (1980).

19) M. Inaba and Z. Ogumi, *Denchi Gijyutu (Battery Technology)*, **8**, 3 (1996).

20) J. R. Dahn, A. K. Sleigh, H. Shi, J. N. Reimers, Q. Zhong, and B. M. Way, *Electrochim. Acta*, **38**, 1179 (1993).

21) M. Inaba, H. Yoshida, and Z. Ogumi, *J. Electrochem. Soc.*, **143**, 2572 (1996).

22) J. Conard and H. Estrade, *Mater. Sci. Eng.*, **31**, 173 (1977).

23) N. Kambe, M. S. Dresselhaus, G. Dresselhaus, S. Basu, A. R. McGhie, and J. E. Fischer, *Mater. Sci. Eng.*, **40**, 1 (1979).

24) K. Tatsumi, A. Mabuchi, N. Iwashita, H. Sakaebe, H. Shioyama, H. Fujimoto, and S. Higuchi, *J. Electrochem. Soc.*, **142**, 716 (1995).

25) C. R. Houska and B. E. Warren, *J. Appl. Phys.*, **25**, 204 (1954).

26) S. Yata, K. Hanefuji, H. Kinoshita, A. Anekawa, T. Hashimoto, K. Tanaka, and T. Yamabe, "Extended Abstracts of 35th Battery Symposium in Japan," Nagoya, Japan, 1994, Abstr., pp. 57—58.

27) K. Sato, M. Noguchi, A. Demachi, N. Oki, and M. Endo, *Science*, **264**, 556 (1994).
28) S. Yata, H. Kinoshita, M. Komori, N. Ando, T. Kashiwamura, T. Harada, K. Tanaka, and T. Yamabe, *Synth. Met.*, **62**, 153 (1994).
29) A. Mabuchi, K. Tokumitsu, H. Fujimoto, and T. Kasuh, *J. Electrochem. Soc.*, **142**, 1041 (1995).
30) T. Zheng, Y. Liu, E. W. Fuller, S. Tseng, U. von Sacken, and J. R. Dahn, *J. Electrochem. Soc.*, **142**, 2581 (1995).
31) T. Zheng, W. R. Mckinnon, and J. R. Dahn, *J. Electrochem. Soc.*, **143**, 2137 (1996).
32) P. Zhou, R. Lee, P. Papanek, C. Bindra, and J. E. Fisher, "Extended Abstracts of 8th International Meeting on Lithium Batteries," Nagoya, Japan, 1996, Abstr., pp. 242—243.
33) T. Zheng, W. R. McKinnon, and J. R. Dahn, *J. Electrochem. Soc.*, **143**, 2137 (1996).
34) N. Sonobe, M. Ishikawa, and T. Iwasaki, "Extended Abstracts of 35th Battery Symposium in Japan," Nagoya, Japan, 1994, Abstr., pp. 47—48.
35) M. Takahashi, M. Ohishi, Y. Mitsuki, M. Yoshimura, K. Shibahara, and S. Sakamoto, "Extended Abstracts of 35th Battery Symposium in Japan," Nagoya, Japan, 1994, Abstr., pp. 39—40.
36) H. Azuma, A. Omaru, H. Imoto, and Y. Nishi, "Extended Abstracts of 58th Annual Meeting of The Electrochemical Society of Japan," Noda, Japan, 1991, Abstr., p. 157.
37) T. Zheng, Q. Zhong, and J. R. Dahn, *J. Electrochem. Soc.*, **142**, L211 (1995).
38) W. Xing, J. S. Xue, T. Zheng, A. Gibaud, and J. R. Dahn, *J. Electrochem. Soc.*, **143**, 3482 (1996).
39) M. Ishikawa, N. Sonobe, H. Nakauma, and T. Iwasaki, "Extended Abstracts of 35th Battery Symposium in Japan," Nagoya, Japan, 1994, Abstr., pp. 49—50.
40) Y. Liu, J. S. Xue, T. Zheng, and J. R. Dahn, *Carbon*, **34**, 193 (1996).
41) a) A. N. Dey and B. P. Sullivan, *J. Electrochem. Soc.*, **117**, 222 (1970); b) G. Eichinger, *J. Electroanal. Chem.*, **74**, 183 (1976); c) M. Arakawa and J. Yamaki, *J. Electroanal. Chem.*, **219**, 273 (1987).
42) R. Fong, U. von Sacken, and J. R. Dahn, *J. Electrochem. Soc.*, **137**, 2009 (1990).
43) a) Z. X. Shu, R. S. McMillan, and J. J. Murray, *J. Electrochem. Soc.*, **140**, L101 (1993); b) Z. X. Shu, R. S. McMillan, and J. J. Murray, *J. Electrochem. Soc.*, **140**, 922 (1993).
44) M. Nagayama, H. Ikuta, T. Uchida, and M. Wakihara, "Extended Abstracts of '95 Fall Meeting of The Electrochemical Society of Japan," Kofu, Japan, 1995, Abstr., p. 162.
45) E. Peled, *J. Electrochem. Soc.*, **126**, 2047 (1979).
46) R. Fong, U. von Sacken, and J. R. Dahn, *J. Electrochem. Soc.*, **137**, 2009 (1990).
47) a) O. Chusid, Y. Ein-Eli, D. Aurbach, M. Babai, and Y. Carmeli, *J. Power Sources*, **43/44**, 47 (1993); b) D. Aurbach, Y. Ein-Eli, O. Chusid, Y. Carmeli, M. Babai, and H. Yamin, *J. Electrochem. Soc.*, **141**, 603 (1994); c) Y. Ein-Eli, B. Markovsky, D. Aurbach, Y. Carmeli, H. Yamin, and S. Luski, *Electrochim. Acta*, **39**, 2559 (1994); d) D. Aurbach, Y. Ein-Eli, B. Markovsky, A. Zaban, S. Luski, Y. Carmeli, and H. Yamin, *J. Electrochem. Soc.*, **142**, 2882 (1995); e) D. Aurbach and Y. Ein-Eli, *J. Electrochem. Soc.*, **142**, 1746 (1995).
48) K. Takai, K. Kumai, Y. Kobayashi, H. Miyashiro, T. Iwahori, T. Uwai, and H. Ue, *J. Power Sources*, **54**, 171 (1995).
49) J. O. Besenhard, M. Winter, J. Yang, and W. Biberacher, *J. Power Sources*, **54**, 228 (1995).
50) a) M. Inaba, Z. Siroma, Z. Ogumi, T. Abe, Y. Mizutani, and M. Asano, *Chem. Lett.*, **1995**, 661; b) M. Inaba, Z. Siroma, A. Funabiki, Z. Ogumi, T. Abe, Y. Mizutani, and M. Asano, *Langmuir*, **12**, 1535 (1996).
51) M. Inaba, Z. Siroma, Y. Kawatate, A. Funabiki, and Z. Ogumi, *J. Power Sources*, in press.
52) a) "Scanning Tunneling Microscopy and Spectroscopy," ed by D. A. Bonnell, VCH, New York (1993); b) R. Wisendanger, "Scanning Probe Microscopy and Spectroscopy," Cambridge University Press, Cambridge (1994); c) "Scanning Tunneling Microscopy I," ed by H.-J. Guntherodt and R. Wisendanger, Springer-Verlag, Berlin (1992).
53) a) S. Morita, S. Tsukada, and J. Mikoshiba, *J. Vac. Sci. Technol., A*, **A6**, 354 (1988); b) D. Tomanek and S. G. Louie, *Phys. Rev., Sect. B*, **B37**, 9327 (1988).
54) R. Setton, "Graphite Interfcalation Compounds I, Structure and Dynamics," ed by H. S. Zabel and A. Solin, Springer-Verlag, Berlin (1990), p. 320.
55) M. Jean, C. Desnoyer, A. Tranchent, and R. Messina, *J. Electrochem. Soc.*, **142**, 2122 (1995).
56) T. Uchida, T. Itoh, Y. Morikawa, H. Ikuta, and M. Wakihara, *Denki Kagaku*, **61**, 1390 (1993).
57) T. Uchida, Y. Morikawa, H. Ikuta, and M. Wakihara, *J. Electrochem. Soc.*, **143**, 2606 (199).
58) N. Takami, A. Satoh, M. Hara, and T. Ohsaki, *J. Electrochem. Soc.*, **142**, 371 (1995).
59) M. Morita, N. Nishimura, and Y. Matsuda, *Electrochim. Acta*, **38**, 1721 (1993).
60) A. Funabiki, M. Inaba, Z. Ogumi, S.-I. Yuasa, J. Ohtsuji, and A. Tasaka, *J. Electrochem. Soc.*, submitted.
61) N. Imanishi, H. Kashiwagi, T. Ichikawa, Y. Takeda, O. Yamamoto, and M. Inagaki, *J. Electrochem. Soc.*, **140**, 315 (1993).
62) A. Funabiki, M. Inaba, and Z. Ogumi, *J. Power Sources*, in press.
63) a) P. C. Eklund, C. H. Olk, F. J. Holler, J. G. Spolar, and E. T. Arakawa, *J. Mater. Res.*, **1**, 361 (1986); b) R. Nishitani, Y. Sasaki, and Y. Nishina, *J. Phys. Soc. Jpn.*, **56**, 1051 (1987); c) R. Nishitani, Y. Sasaki, and Y. Nishina, *Phys. Rev., Sect. B*, **B37**, 3141 (1988).
64) a) G. Scholz, P. Joensen, J. M. Reyes, and R. F. Frindt, *Physica, B (Amsterdam)*, **B105**, 214 (1981); b) D. Kaluarachchi and R. F. Frindt, *Phys. Rev., Sect. B*, **B28**, 3663 (1983); c) G. R. Carlow, P. Joensen, and R. F. Frindt, *Phys. Rev., Sect. B*, **B42**, 1124 (1990).
65) T. Kasuh, A. Mabuchi, K. Tokumitsu, and H. Fujimoto, "Extended Abstracts of 8th International Meeting on Lithium Batteries," Nagoya, Japan, 1996, p. 97.

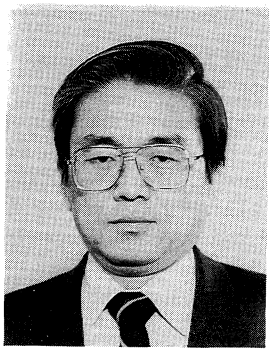

Zempachi Ogumi, Dr. of Eng., Professor of Graduate School of Engineering, Kyoto University: born in 1945 in Tokushima, Japan, studied chemistry at Kyoto University under Prof. Shiro Yoshizawa. After finishing his work for dissertation, he worked at Fritz-Haber institut der Max-Planck Gesellschaft in Berlin for 1 year and since then he has been working in the field of electrochemistry with Prof. Yoshizawa and Prof. Zen-ichiro Takehara at Kyoto University. His current research interests include electrochemistry: in particular, preparation, characterization, and reactions of materials for batteries and fuel cells, and solid state ionics.

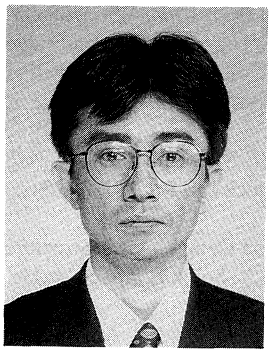

Minoru Inaba, Dr. of Eng., Instructor of Graduate School of Engineering, Kyoto University: born in 1961 in Shizuoka, Japan, studied chemistry at Kyoto University under Prof. Zen-ichiro Takehara. After he graduated from the master's course, he worked for Tokuyama Co., Ltd. for 6 years. After leaving the company, he has been working in the field of electrochemistry with Prof. Zempachi Ogumi at Kyoto University. His current research interests include in situ measurements, in particular, using Raman spectroscopy and STM, of electrode/electrolyte interfaces in electrochemical reactions. He is now staying at Lawrence Berkeley National Laboratory, University of California, Berkeley, CA, USA to work with Dr. Frank McLarnon and Dr. Kim Kinoshita on active materials in lithium batteries.